HIGH-RESOLUTION INFRARED MEASUREMENTS OF H₂O AND SiO IN SUNSPOTS

G. SONNABEND

[1]*NASA Goddard Space Flight Center, Greenbelt, MD, U.S.A.*
(e-mail: gsonnabend@lepvax.gsfc.nasa.gov)

D. WIRTZ

Philips Research Laboratories, Hamburg, Germany

R. SCHIEDER

KOSMA, University of Cologne, Köln, Germany

and

P. F. BERNATH

Department of Chemistry, University of Waterloo, Waterloo, ON, Canada

Abstract. Ultra-high-resolution spectroscopic measurements ($R \approx 10^7$) of water vapor and silicon monoxide in sunspots are presented. Observations were performed using the Cologne Tunable Heterodyne Infrared Spectrometer (THIS) at the McMath–Pierce Solar Observatory. Mid-infrared molecular absorption lines around 10 μm were recorded and resolved in full detail. The linewidth and shape can thus be determined with high precision and were used to calculate kinetic temperatures which are much higher than the physical temperatures of the sunspot.

1. Introduction

Molecular features in sunspots have been observed for many years. Measurements of linewidths can provide valuable information, e.g., on the temperature and the dynamics of the observed solar region. In the mid-infrared wavelength region around 1000 cm^{-1} the most prominent molecular features stem from highly excited molecules like SiO and H₂O. Many observations of these molecules have been carried out by Fourier transform (FT) spectroscopy of the Sun and in the laboratory (see e.g., Wallace *et al.*, 1995, 1996; Campbell *et al.*, 1995). Nevertheless the frequency resolution of FT spectrometers (FTS) in the mid-IR is typically limited to about 150 MHz.

Using the heterodyne technique, the frequency resolution can be improved by more than one order of magnitude and line profiles can be analyzed in full detail. IR-heterodyne systems using a gas laser for the local oscillator (LO) are fixed in frequency and, given a usable detector bandwidth of typically 1.5 GHz, the overall frequency coverage of these systems is rather poor.[1] Using tunable LOs like

---

[1] Only 15% of the wavelengths between 9 and 12 μm can be covered using CO₂ and all its isotopologues as laser gases (Kostiuk and Mumma, 1983).

tunable diode lasers (TDLs) full coverage of the mid-IR is theoretically possible but the sensitivity of TDL-based instruments is typically worse by a factor of 5–10 compared to gas laser instruments due to the rather poor single mode power available from these lasers (Ku and Spears, 1977; Glenar *et al.*, 1982; Fukunishi *et al.*, 1990; McElroy *et al.*, 1990). This is important especially for astrophysical observations since sources are typically fainter by a factor of more than 10^3 compared to the Sun. Nevertheless infrared-heterodyne observations of molecules in sunspots have been carried out successfully in the past with TDL-based heterodyne systems (Glenar *et al.*, 1983).

Recently, the use of quantum cascade lasers (QCLs) (Faist *et al.*, 1994; Beck *et al.*, 2002) in our system led to a breakthrough giving the Cologne Tunable Heterodyne Infrared Spectrometer (THIS) a sensitivity equal to gas laser-based heterodyne receivers without losing the tunability. Along with a QCL as LO, the instrument incorporates a fast mercury cadmium telluride (MCT) detector as a mixer-detector, some optics to match the receiver to the telescope and to superimpose the LO and telescope beams, and a 2048-channel (1.4 GHz) acousto-optical spectrometer (AOS) for instantaneous multichannel frequency analysis (Schieder, Tolls, and Winnewisser, 1989). A detailed description of the system can be found in (Schmülling *et al.*, 1998) and (Sonnabend *et al.*, 2002). Due to the multiplex advantage of the AOS a sufficient signal-to-noise ratio (SNR) can be reached in seconds when observing bright objects like the Sun. THIS is being developed for astrophysical studies and is planned for use on board the stratospheric observatory *SOFIA*.

2. Measurement Procedure and Calibration

The operation of THIS proceeds by making a sequence of four measurements as described below and the spectrum of an object is given by

$$J = \frac{S_i - R_i}{H_i - C_i}(J_{\mathrm{H}} - J_{\mathrm{C}}), \tag{1}$$

in which S, R, H, and C denote the counts taken by the AOS for looking on (signal)/off (reference) the source, on a (hot) calibration load, and on an ambient temperature (cold) load in a given time interval. The index i stands for the frequency pixel of the spectrometer and will be omitted in the following. Taking the difference of counts in the numerator removes the background counts generated in the spectrometer and dividing by the blackbody differences corrects for the uneven gain of the receiver across the intermediate frequency (IF) band. The differences in the count rates are directly proportional to the differences in (brightness) temperatures of the different radiation sources.

The factor $(J_{\mathrm{H}} - J_{\mathrm{C}})$ (in K) provides the temperature calibration using the known temperatures of the calibration loads. Since we operate at rather high frequencies,

the brightness temperatures of the two loads J_H and J_C are to be calculated from Planck's radiation formula

$$J_x = \frac{h\nu_{Obs}}{k_B}\left(\exp\left(\frac{h\nu_{Obs}}{k_B T_{Phys}}\right) - 1\right)^{-1},$$ (2)

with their physical temperatures T_{Phys} and the observed frequency ν_{Obs} as parameters. Equation (1) thus directly provides the brightness temperature difference between the signal and reference position as seen by the detector including all losses, e.g., in the receiver and telescope optics. See Schmülling *et al.* (1998) and Sonnabend *et al.* (2002) for further information on calibration of the measured spectra.

What needs to be considered in detail is the usually unknown impact of the atmosphere that is still included in the source measurements (S, R). In order to measure the atmospheric transmission at the observing wavelength as well as the coupling efficiency of the receiver to the telescope we recorded the observed temperature of the undisturbed Sun at various airmasses during the day (a method known in radio astronomy as 'skydip'). From those numbers the atmospheric and instrumental contributions to the signal loss were calculated.

For the observations discussed here, a calibrated blackbody source with a physical temperature of 673 K and an emissivity of 95% was used so that $(J_H - J_C)$ equals $(169 \times 0.95) - 7 = 153$ K at 1089 cm^{-1} or 9.18 μm wavelength. The physical temperature of the solar photosphere of 5870 K results in a brightness temperature of 5120 K using Equation (2) for all calculations.

3. Measurements

3.1. ATMOSPHERE AND COUPLING

The atmospheric transmission from skydip measurements yielded about 95%, which fits to theoretical values generated by calculating the atmospheric radiative transfer using the HITRAN database.

The telescope coupling efficiency was calculated to $66.5 \pm 2\%$. This has to be compared with the theoretical main-beam efficiency of 88% for the receiver–telescope setup when observing the Sun or any other extended object. For calculating the main-beam efficiency telescope illumination, an optimal Gaussian beam (edge taper of 10.9 dB, see Goldsmith, 1998) is assumed. The difference can be attributed to losses in the telescope optics and some unknown mismatch between receiver and telescope. The coupling efficiency results in an effective brightness temperature difference between solar photosphere and blank sky observable with the given setup (in absence of the atmosphere) of 3235 K instead of the expected
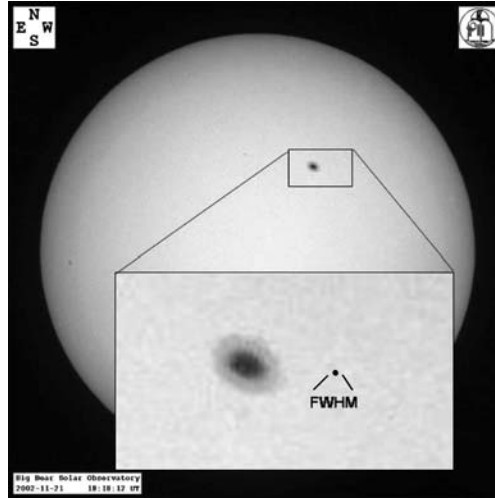
Figure 1. An image of the Sun from November 21, 2002. This is the sunspot for which the measurements were carried out and the FWHM of the telescope beam is shown in the inset. (Picture taken from the website of the Big Bear Solar Observatory operated by the New Jersey Institute of Technology.)

5120 K.[2] The errors for the opacity and the maximum detectable brightness temperature difference are about 10%.

3.2. SiO AND H_2O IN SUNSPOTS

From November 17 to December 2, 2002 THIS was installed at the west auxiliary telescope of the McMath–Pierce Solar Observatory on Kitt Peak. Measurements of sunspots were carried out on November 20–21, 2002.

A picture of the Sun with the observed sunspot marked is shown in Figure 1. We observed the Sun with a rather small telescope beam of roughly 6 arc s full width at half maximum (FWHM) as shown in the inset. One way of measuring the molecular features in the sunspot and at the same time removing atmospheric features (mostly ozone) contaminating the spectra would have been to record the following:

$$T_S = \frac{S_{spot} - R_{sky}}{S_{sun} - R_{sky}} \times (J_{sun} - J_{sky}). \tag{3}$$

Equation (3) directly yields antenna temperatures T_S, i.e., detected brightness temperature differences corrected for atmospheric influences and all receiver and coupling losses. Since the receiver optics and the telescope did not allow beam-switching between spot and blank sky during one measurement cycle, a cold load measurement was recorded instead of the blank sky. Doing so results in small

[2]Since measurements with THIS are always carried out as on/off measurements only differences in brightness temperatures are discussed here instead of temperatures of single sources.

residuals due to stratospheric ozone in the final spectrum, which can be removed almost completely by introducing a constant correction factor ϵ. The spectra were thus recorded in the following way:

$$T_S = \frac{S_{spot} - (R_{cold} - \epsilon)}{R_{sun} - (R_{cold} - \epsilon)} \times (J_{sun} - J_{cold}) \tag{4}$$

and ϵ varied between 0.015 and 0.04%.

Applying Gaussian error propagation in combination with the radiometer equation to the measurement cycle used here (see Equation (4)) allows us to compare the measured rms noise to the best case possible, that is to the purely radiometric behavior of the system (Sonnabend *et al.*, 2002). Table I shows the results. While performing our measurements, the operation of THIS was nearly purely radiometric. The resulting differences can be attributed to thermal effects because part of the receiver was exposed to sunlight in the focal plane of the telescope.

Examples of molecular features in sunspots measured with THIS are shown in Figures 2 and 3. The observing time was 73 s (Figure 2) and 670 s (Figure 3).

TABLE I

Comparison of measured and calculated rms noise for the measurements shown.

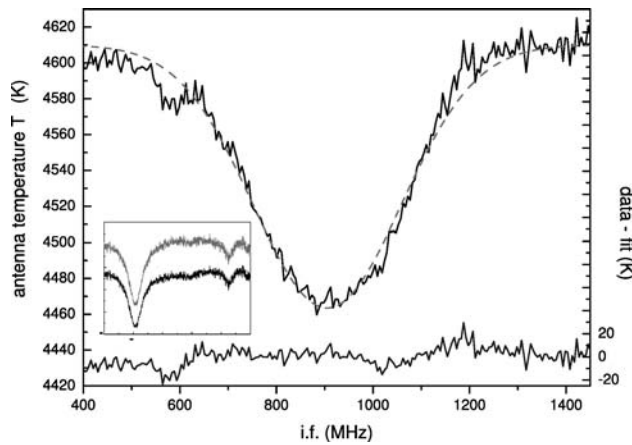| Molecule	Transition	Measured rms noise (K)	Theoretical rms noise (K)
^{28}SiO	6–5 P(50)	4.35	4.30
H_2O	040–030 $15_{1,15}-15_{2,14}$	1.76	1.38

Figure 2. ^{28}SiO 6–5 P(50) absorption at 1088.8093 cm^{-1}. Plotted is the antenna brightness temperature at the observation wavelength against the intermediate frequency. Also shown is a Gaussian fit to the data and the resulting residuals. In the inset, the uncalibrated spectra taken on(*black*)/off(*gray*) the sunspot are shown.
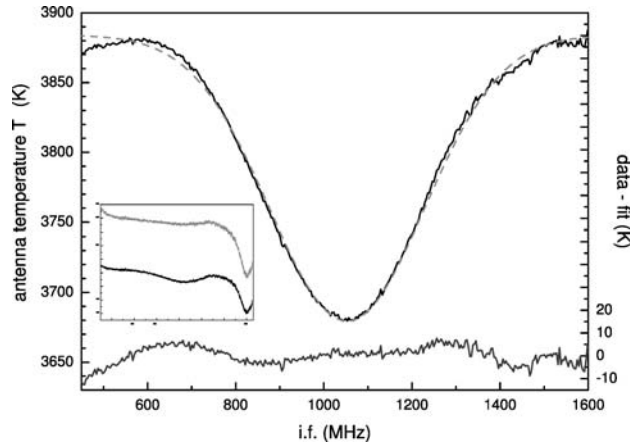
Figure 3. H_2O 040–030 $15_{1,15}$–$15_{2,14}$ absorption at 1088.9251 cm^{-1}. Plotted is the antenna brightness temperature at the observation wavelength against the intermediate frequency. Also shown is a Gaussian fit to the data and the resulting residuals. In the inset, the uncalibrated spectra taken on(*black*)/off(*gray*) the sunspot are shown.

Both spectra are binned to a 5 MHz frequency resolution. The insets show that the uncalibrated spectra on/off the spot are still heavily contaminated with stratospheric ozone absorptions. The line assignments were carried out by using the infrared spectral atlases of the Sun (Wallace *et al.*, 1996).

The difference in the background (continuum) temperature between the two measurements probably arises from pointing inaccuracies while tracking the sunspot which caused the beam occasionally to be partly on the undisturbed Sun. Therefore, the shown values are upper limits. For Figures 2 and 3 the given antenna temperatures for the continuum of 4600 and 3870 K correspond to physical temperatures of 5180 and 4445 K for the sunspot, respectively. From the depth of the absorption lines upper limits for the temperatures of the absorbing gas are calculated to be 5038 and 4254 K, respectively. Table II shows the measured line frequencies and widths. The Doppler formula (Bernath, 2005),

$$\Delta \nu_D = \frac{\nu_0}{c} \sqrt{\frac{8kT \ln(2)}{m}}, \tag{5}$$

was used to relate the observed Doppler widths $\Delta \nu_D$ (FWHM) to the effective temperature T of the species of molecular weight m. The LO frequency scale was calibrated using the SiO (Campbell *et al.*, 1995) and H_2O (Zobov *et al.*, 1999) line positions reported previously. The previous measurements (Campbell *et al.*, 1995) of the SiO line in a large sunspot by Wallace *et al.* (1996) and Campbell *et al.* (1995) with the Kitt Peak FTS gave a value of 550 MHz for the linewidth as compared to 358 MHz obtained with THIS. For the water line at 1088.9251 cm^{-1} the linewidth

TABLE II

Measured line positions and widths.

Molecule	Transition	Frequency (cm^{-1})	Linewidth (MHz)	Temperature (K)
^{28}SiO	6–5 P(50)	1088.8095	358 ± 11	10347 ± 635
H_2O	040–030 $15_{1.15}$–$15_{2.14}$	1088.9251	406 ± 9	5442 ± 241

in the sunspot was measured to be 566 MHz with the FTS. Our observation yielded 406 MHz. Given that the FTS had a much lower spectral resolution, the new values are in reasonable agreement with the previous measurements and illustrate the higher resolution available with THIS.

It is obvious that the determined kinetic temperatures exceed typical physical temperatures of medium-sized sunspots (<4000 K) by far. The kinetic temperatures determined for SiO are even higher than the photospheric solar temperature. The H_2O value exceeds the thermal dissociation temperature for the water molecule.

These findings suggest that a large part of the observed Doppler width is not due to simple thermal excitation. In the past, these non-thermal line broadening effects were ascribed empirically to microscopic and macroscopic turbulence in the solar photosphere (Gray, 1978). The idea is that there is extra broadening due to turbulence at the molecular level and also due to macroscopic motion of hot gas cells (i.e., granulation on the Sun). These ideas are now obsolete (Asplund *et al.*, 2000) because realistic three-dimensional simulations of radiation and convection in solar photosphere can account quantitatively for experimental observations of line shapes and line shifts. Asplund *et al.* show that non-thermal line broadening is due to Doppler shifts arising from convective flows and solar oscillations. Magnetic fields cannot be responsible for the extra broadening because both SiO and H_2O are closed-shell species with no net orbital or spin angular momentum. Unlike for other molecules like OH, the Zeeman effect is very small and does not make a measurable contribution.

The non-thermal and thermal contributions to the linewidth are proportional to frequency so observations of detailed solar line shapes are easier in the near infrared and visible regions. The high resolution, sensitivity, and tunability of heterodyne spectroscopy with QCLs allows these kind of observations to be carried out for other objects as well as the Sun.

4. Conclusion

Heterodyne instruments allow a very detailed look at processes in the solar atmosphere. Since line profiles can be analyzed in complete detail, the effects of

dynamics, magnetic fields, or pressure (e.g., Dicke-narrowing) on those molecules can be investigated with high accuracy. With the upcoming of large solar telescopes (GREGOR, ATST) also small-scale variations of these parameters can be studied.

Using QCLs as LOs allowed us to build a transportable and tunable IR heterodyne receiver, which operates with sensitivities equal to gas laser-based instruments and that can be used on all kinds of telescopes.

The presented measurements of molecular features in sunspots also offer interesting perspectives to observations of similar features in stellar atmospheres.

Acknowledgements

References

Asplund, M., Nordlund, A., Trampedach, R., Allende Prieto, C., and Stein, R. F.: 2000, *Astron. Astrophys.* **359**, 729.

Beck, M., Hofstetter, D., Aellen, T., Faist, J., Oesterle, U., Ilegems, M., Gini, E., and Melchior, H.: 2002, *Science* **295**, 301.

Bernath, P.: 2005, *Spectra of Atoms and Molecules*, 2nd edn., Oxford University Press, Oxford.

Campbell, J. M., Klapstein, D., Dulick, M., and Bernath, P.: 1995, *Astrophys. J. Suppl.* **101**, 237.

Faist, J., Capasso, F., Sivco, D. L., Sirtori, C., Hutchinson, A. L., and Cho, A. Y.: 1994, *Science* **264**, 553.

Fukunishi, H., Okano, S., Taguchi, M., and Ohnuma, T.: 1990, *Appl. Opt.* **29**, 2722.

Glenar, D., Kostiuk, T., Jennings, D. E., Buhl, D., and Mumma, M. J.: 1982, *Appl. Opt.* **21**(2), 253.

Glenar, D. A., Deming, D., Jennings, D. E., Kostiuk, T., and Mumma, M. J.: 1983, *Astrophys. J.* **269**, 309.

Goldsmith, P. E.: 1998, *Quasioptical Systems – Gaussian Beam Quasioptical Propagation and Applications*, IEEE Press, Piscataway, NJ.

Gray, D. F.: 1978, *Solar Phys.* **59**, 193.

Kostiuk, T. and Mumma, M. J.: 1983, *Appl. Opt.* **22**(17), 2644.

Ku, R. T. and Spears, D. L.: 1977, *Opt. Lett.* **1**(3), 84.

McElroy, C. T., Goldman, A., Fogal, P. F., and Murcray, D. G.: 1990, *J. Geophys. Res.* **95**(D5), 5567.

Schieder, R., Tolls, V., and Winnewisser, G.: 1989, *Exp. Astron.* **1**, 101.

Schmülling, F., Klumb, B., Harter, M., Schieder, R., Vowinkel, B., and Winnewisser, G.: 1998, *Appl. Opt.* **37**, 5771.

Sonnabend, G., Wirtz, D., Schmülling, F., and Schieder, R.: 2002, *Appl. Opt.* **41**(15), 2978.

Wallace, L., Bernath, P., Livingston, W., Hinkle, K., Busler, J., Guo, B., and Zhang, K.: 1995, *Science* **268**, 1155.

Wallace, L., Livingston, W., Hinkle, K., and Bernath, P.: 1996, *Astrophys. J. Suppl.* **106**, 165.

Zobov, N. F., Polyansky, O. L., Tennyson, J., Lotoski, J. A., Colarusso, P., Zhang, K.-Q., and Bernath, P. F.: 1999, *J. Mol. Spectrosc.* **193**, 118.